

# DeepMTS: Deep Multi-task Learning for Survival Prediction in Patients with Advanced Nasopharyngeal Carcinoma using Pretreatment PET/CT

Mingyuan Meng <sup>a,1</sup>, Bingxin Gu <sup>b,1</sup>, Lei Bi <sup>a,\*</sup>, Shaoli Song <sup>b</sup>, David Dagan Feng <sup>a</sup>, and Jinman Kim <sup>a,\*</sup>

<sup>a</sup> School of Computer Science, the University of Sydney, Sydney, Australia.

<sup>b</sup> Department of Nuclear Medicine, Fudan University Shanghai Cancer Center; Department of Oncology, Shanghai Medical College, Fudan University; Center for Biomedical Imaging, Fudan University; Shanghai Engineering Research Center of Molecular Imaging Probes; Key Laboratory of Nuclear Physics and Ion-beam Application (MOE), Fudan University; Shanghai, PR China.

**Abstract** — Nasopharyngeal Carcinoma (NPC) is a worldwide malignant epithelial cancer. Survival prediction is a major concern for NPC patients, as it provides early prognostic information that is needed to guide treatments. Recently, deep learning, which leverages Deep Neural Networks (DNNs) to learn deep representations of image patterns, has been introduced to the survival prediction in various cancers including NPC. Deep survival models using DNNs can directly predict the survival outcomes of patients from image input in an end-to-end manner. It has been reported that image-derived end-to-end deep survival models have the potential to outperform clinical prognostic indicators and traditional radiomics-based survival models in prognostic performance. However, deep survival models, especially 3D models, require large image training data to avoid overfitting. Unfortunately, medical image data is usually scarce, especially for Positron Emission Tomography/Computed Tomography (PET/CT) due to the high cost of PET/CT scanning. Compared to Magnetic Resonance Imaging (MRI) or Computed Tomography (CT) providing only anatomical information of tumors, PET/CT that provides both anatomical (from CT) and metabolic (from PET) information is promising to achieve more accurate survival prediction. However, we have not identified any 3D end-to-end deep survival model that applies to small PET/CT data of NPC patients. In this study, we introduced the concept of multi-task leaning into deep survival models to address the overfitting problem resulted from small data. Tumor segmentation was incorporated as an auxiliary task to enhance the model's efficiency of learning from scarce PET/CT data. Based on this idea, we proposed a 3D end-to-end Deep Multi-Task Survival model (DeepMTS) for joint survival prediction and tumor segmentation. Our DeepMTS can jointly learn survival prediction and tumor segmentation using PET/CT data of only 170 patients with advanced NPC. Our DeepMTS was tested on an external testing set enrolling 23 advanced NPC patients acquired from different centers and consistently outperformed traditional radiomics-based survival models and existing deep survival models.

**Keywords** — Deep multi-task learning, Survival prediction, PET/CT, Nasopharyngeal carcinoma.

## 1. Introduction

Nasopharyngeal Carcinoma (NPC) is a worldwide malignant epithelial cancer that arises from the nasopharynx epithelium, especially the fossa of Rosenmüller [1]. According to the GLOBOCAN 2020 published by the International Agency for Research on Cancer (IARC), there are approximately 133,354 new NPC patients and 80,008 NPC-related deaths worldwide in 2020 [2]. Survival prediction is a major concern for NPC patients, as it provides early prognostic information that is needed to guide treatments. Survival prediction is a regression task that models the survival outcomes of patients. However, compared to typical regression tasks such as

\* Corresponding authors.

<sup>1</sup> Mingyuan Meng and Bingxin Gu contributed equally to this work.

Emails address: lei.bi@sydney.edu.au (L. Bi) and jinman.kim@sydney.edu.au (J. Kim)

clinical score prediction [3], survival prediction is more challenging as it has to handle right-censored survival data in which the time of events occurring is unclear for some patients (e.g., patients may be lost to follow-up).

The Tumor, Node, Metastasis (TNM) staging system from American Joint Committee on Cancer (AJCC)/Union for International Cancer Control (UICC) is widely used to predict the survival outcomes and guide the treatments for NPC patients [4]. However, the TNM stage only provides limited benefit for prognoses in patients with advanced NPC. Large variations have been reported on the survival outcomes of the patients classified into the same TNM stage and receiving similar treatments [5][6][7]. This may be attributed to the fact that the TNM stage only takes into account the anatomical information derived from Magnetic Resonance Imaging (MRI) or Computed Tomography (CT). Multi-modality imaging of Positron Emission Tomography/Computed Tomography (PET/CT), providing both anatomical (from CT) and metabolic (from PET) information of tumors, is promising to achieve more accurate survival prediction. Conventional PET/CT parameters, including Standardized Uptake Value (SUV), Metabolic Tumor Volume (MTV), and Total Lesion Glycolysis (TLG), have been reported as individual prognostic indicators for survival prediction in advanced NPC. However, they failed to represent intra-tumor information such as tumor texture, intensity, heterogeneity, and morphology [8][9][10], thereby resulting in suboptimal survival prediction.

Radiomics, as a widely recognized computational method for prognosis, refers to the extraction and analysis of high-dimensional quantitative features from medical images [11]. It has drawn much attention among clinical oncologists due to its ability to provide comprehensive representations of tumor characteristics, including intra-tumor information [12]. The common pipeline of radiomics for survival prediction consists of (1) image acquisition and reconstruction, (2) manual segmentation of tumor regions, (3) extraction of handcrafted radiomics features and, (4) statistical analysis of radiomics features using traditional survival models (e.g., the Cox proportional hazards model [13]). Radiomics has been widely used for survival prediction in various cancers including NPC [12][14][15]. However, radiomics is heavily dependent on human prior knowledge such as manual segmentation, handcrafted feature extraction, and manual tuning of survival model parameters, so its limitations in bringing a source of human bias and lacking the ability to understand high-level semantic information have been well recognized [16][17].

Recently, deep learning, which leverages Deep Neural Networks (DNNs) to learn deep representations of image patterns, has been used for survival prediction in various cancers including NPC [17][18][19]. There mainly exist three approaches of using deep learning for survival prediction: (1) DNNs replace the traditional survival models in the radiomics pipeline to model handcrafted features [20]. (2) Pretrained DNNs are used to extract deep features, which can enhance or even replace handcrafted features for radiomics analysis [18][21][22]. (3) DNNs are trained to directly predict survival outcomes from image input, in which the feature extraction and feature analysis are jointly learned in an end-to-end manner [19][23][24]. It has been reported that end-to-end deep survival models (the 3<sup>rd</sup> approach) outperformed the 1<sup>st</sup> and 2<sup>nd</sup> approaches for survival prediction in some cancers [19][23]. End-to-end deep survival models usually do not require manual segmentation of tumor regions and allow for automatic learning of relevant and robust features without human intervention. Therefore, they can remove the human bias introduced by manually segmented tumor regions and handcrafted features, and potentially discover high-level semantic features that may be overlooked by manually-defined feature extraction [25]. However, end-to-end deep survival models usually require large image training data to avoid overfitting, especially for 3D deep models [19][24]. Compared to 2D models, 3D models can make predictions based on the whole 3D tumor regions, but they have more learnable parameters and thereby require more training data. Unfortunately, due to the high cost of PET/CT scanning, routine diagnostic/prognostic imaging for NPC patients usually is MRI. Therefore, PET/CT data of NPC patients is limited. In this study, we aim to establish a 3D end-to-end deep survival model that applies to small PET/CT data.

To address the overfitting problem resulted from small data, we introduced the concept of multi-task learning into deep survival models. Multi-task learning is a subfield of machine learning in which multiple tasks are simultaneously learned by a shared model [26]. This approach improves data efficiency and reduces overfitting by leveraging the shared features learned for multiple tasks [27]. Recently, we identified that tumor segmentation has been used as an auxiliary task in deep multi-task learning and benefited tumor-related tasks such as glioma diagnosis [28], genotype prediction [29], and treatment response prediction [30]. This is likely because

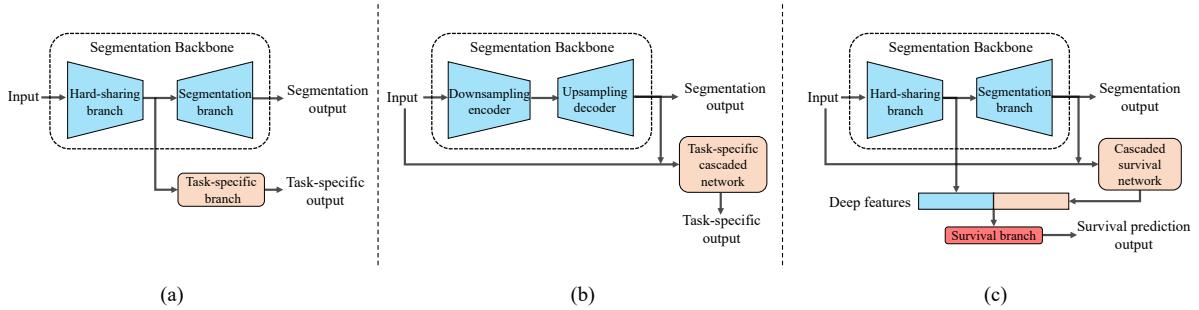


Fig. 1. A conceptual illustration of (a) hard-sharing multi-task architectures, (b) cascaded multi-task architectures, and (c) a hybrid multi-task architecture used in the proposed DeepMTS for joint survival prediction and tumor segmentation.

the tumor segmentation task can guide the model to extract the features related to tumor regions [30]. Since survival prediction also is highly relevant to tumor characteristics, we anticipated that the survival prediction task can benefit from the tumor segmentation task as well. Moreover, deep segmentation models can work with small training data (even less than 50 images) [31][32], which suggests that segmentation losses have high efficiency in leveraging small data. Therefore, combining tumor segmentation as an auxiliary task is promising to achieve more accurate survival prediction, especially when using small PET/CT data of NPC patients.

In this study, we proposed a 3D end-to-end Deep Multi-Task Survival model (DeepMTS) for joint survival prediction and tumor segmentation. Our DeepMTS can jointly learn survival prediction and tumor segmentation using PET/CT data of only 170 patients. Tumor segmentation, as an auxiliary task, enhance the DeepMTS to effectively learn from scarce PET/CT data. For survival prediction, the DeepMTS predicted the risk of disease progression, which is a regression task where a higher predicted risk value indicates a patient with shorter Progression-Free Survival (PFS). Our training set enrolled 170 patients with advanced NPC. The DeepMTS was trained and validated through 5-fold cross-validation within the training set, and then was tested on an external testing set enrolling 23 advanced NPC patients acquired from different centers. Our DeepMTS was extensively compared with radiomics-based traditional survival models and existing deep survival models. The experimental results show that our DeepMTS outperformed all comparison methods for the survival prediction in NPC patients.

Based on our review, our DeepMTS is the first deep model incorporating deep multi-task learning for image-derived survival prediction. Moreover, our DeepMTS differs from existing deep multi-task models in architecture designs. Traditionally, most multi-task models in computer vision used simple hard-sharing multi-task architectures: A hard-sharing branch extracts common features shared by all tasks and then is followed by multiple task-specific output branches [27]. For deep multi-task models combining segmentation and other tasks, in most cases [28][33][34], a segmentation network (U-Net [31] or its extensions) was used as a backbone, in which the downsampling encoder was used as the hard-sharing branch followed by multiple task-specific output branches (Fig. 1a). Besides, cascaded multi-task architectures have also been used for joint segmentation and classification [29][35]. In this architecture, the output of the segmentation backbone, as auxiliary information, was fed into a task-specific cascaded network for classification, and the two networks were trained cooperatively in an end-to-end manner (Fig. 1b). Our DeepMTS used a hybrid multi-task architecture: the DeepMTS can derive deep features from both the hard-sharing branch and a cascaded survival network. The features derived from these two parts are complementary to facilitate survival prediction (Fig. 1c). Furthermore, we used a self-designed segmentation network as the backbone. Compared to the widely used U-net [31], our self-designed segmentation network showed much higher learning efficiency and contributed to better performance on survival prediction.

## 2. Related Work

### 2.1. Traditional Survival Models

The Cox Proportional Hazards (CPH) model [13] is the most widely used survival model in medical applications, but it makes strong assumptions about the underlying stochastic process and the relationship between prognostic factors and survival outcomes, resulting in difficulties in exploring complex relationships between prognostic factors and survival outcomes [36]. So far, the CPH model has been extended to many variants such as Lasso-Cox [37], EN-Cox [38], and Transfer-Cox [39]. Lasso-Cox and EN-Cox use Least Absolute Shrinkage and Selection Operator (LASSO) regression and elastic-net penalizations for feature selection, respectively. Transfer-Cox is a transfer learning method for survival analysis via efficient L2/1-norm regularized Cox regression.

There exist other survival models that make different assumptions from CPH-based survival models. For example, Shivaswamy et al. [40] proposed a Support Vector Machine (SVM) approach to model right-censored survival data, and Van Belle et al. [41] proposed a least-squares SVM approach that uses ranking and regression loss. Moreover, recently developed survival models include Random Survival Forest (RSF) [42], Boosting Concordance Index (BoostCI) [43], and Multi-Task Learning model for Survival Analysis (MTLSA) [44]. RSF is a tree model that generates an ensemble estimate for survival data. BoostCI is a survival model in which the concordance index metric is seen as an equivalent smoothed criterion using the sigmoid function. MTLSA reformulates the survival analysis problem as a multi-task learning problem to estimate the survival status at each time interval during the study duration. These survival models can achieve competitive results with traditional Cox-based survival models.

The traditional survival models cannot directly apply to image data. Therefore, image-derived handcrafted radiomics features are necessary in the traditional survival analysis pipeline. However, the manually-defined feature extraction process brings a source of human bias and lacks the ability to understand high-level semantic information [17].

### 2.2. Deep Learning for Survival Prediction

Early studies of deep learning for survival prediction focus on learning the nonlinear relationships between clinical prognostic indicators and survival outcomes. Faraggi et al. [45] first proposed to use a neural network under the CPH assumptions for survival prediction. But their model failed to outperform the CPH model because the practice of neural networks was not as developed as it is today. Until a few years ago, Katzman et al. [46] incorporated modern deep learning techniques into Faraggi et al. [45]'s model and proposed a CPH-based deep survival model (DeepSurv) with a Cox negative logarithm partial likelihood loss. Gensheimer et al. [47] discarded the CPH assumptions and proposed a discrete-time survival model to directly predict conditional probability of patients surviving on each time interval. These models cannot directly apply to image data as well.

As for image-derived survival prediction, Matsuo et al. [20] proposed to use a DNN to model hand-crafted radiomics features for survival prediction in cervical cancer. Lao et al. [21] and Cui et al. [22] used Convolutional Neural Networks (CNNs) to extract deep features and then adopted Cox-based traditional survival model for survival prediction in Glioblastoma Multiforme and lung cancer, respectively. These methods adopted DNNs for image-derived survival prediction, but they failed to directly predict the survival outcomes from image input in an end-to-end manner.

Recently, Zhang et al. [23] proposed an 2D end-to-end CNN-based survival model (CNN-Survival) for survival prediction in pancreatic ductal adenocarcinoma using CT images. This model outperformed the radiomics-based CPH model, but it's still far from optimal because it made prediction based on only one single slice and thus lost the prognostic information existing in 3D tumor volumes. Kim et al. [24] proposed an 3D end-to-end Deep Learning survival Prediction Model (DLPM) for lung adenocarcinomas. This 3D model got rid of the limitations of 2D models, but it was trained with a large dataset including 640 patients and cannot apply to our small PET/CT data of 170 NPC patients.

### 2.3. Survival Prediction in Patients with NPC

Image-derived survival prediction has been explored for patients with NPC [14][15]. Zhang et al. [14] explored the survival prediction in NPC patients using multi-parametric MRI. In their study, handcrafted radiomics features were extracted from MRI images and then were used to build a Lasso-Cox model. Lv et al. [15] explored the survival prediction in NPC patients using PET/CT. Similarly, they also extracted handcrafted radiomics features from PET/CT images. The most prognostic features were selected by univariate Cox analysis and then were used to build a CPH model.

Recently, deep learning has also been used for survival prediction in patients with NPC [18][19]. Peng et al. [18] proposed the earliest studies where deep learning was introduced into the survival prediction in NPC patients. They used a pre-trained 2D CNN to extract deep features from PET and CT slices separately and then fed the deep features and handcrafted radiomics features into a Lasso-Cox model to establish a prognostic nomogram. Their study suggested that deep features can serve as reliable and powerful indicators for survival prediction in NPC patients. Subsequently, Jing et al. [19] proposed the first 3D end-to-end deep model for survival prediction in NPC patients. It is a Multi-modality Deep Survival Network (MDSN) that directly predicts the risk of disease progression from pretreatment MRI. Their study demonstrated that end-to-end deep survival models are more effective to extract relevant features and showed higher prognostic performance. However, the training of MDSN relied on a very large MRI dataset including 1417 NPC patients. From our review, we have not identified any 3D end-to-end deep survival model that applies to our small PET/CT dataset including 170 NPC patients.

### 2.4. Deep Multi-task Learning for Medical Image Analysis

For medical image analysis, deep multi-task learning has been recently explored in the tasks of segmentation and classification. Xue et al. [28] proposed a radiomics-enhanced multi-task neural network for joint glioma subtyping and segmentation using MRI. Liu et al. [29] proposed a cascaded CNN for joint segmentation and genotype prediction of brainstem gliomas using MRI as well. Jin et al. [30] proposed a deep multi-task model to simultaneously perform tumor segmentation and treatment response prediction using pre- and post-treatment MRI. Amyar et al. [33] proposed a deep multi-task model to jointly identify COVID-19 patients and segment lesions from chest CT. Mehta et al. [35] proposed a deep multi-task model for joint segmentation and classification for diagnosis of breast biopsy images.

For regression tasks, Cao et al. [34] proposed a multi-task neural network for joint hippocampus segmentation and regression of mini-mental state examination score using MRI. As we have already mentioned, survival prediction is also a regression task, but it is usually regarded as a more challenging problem because it has to handle right-censored survival data. Currently, we have not identified any deep multi-task model proposed for image-derived survival prediction.

## 3. Method

### 3.1. Overview

We used the DeepMTS to directly predict the risk of disease progression from PET/CT input in an end-to-end manner. Fig. 2 shows the workflow of the proposed DeepMTS. The whole workflow takes as input a pair of preprocessed 3D PET/CT images ( $128 \times 128 \times 112$ ; see Section 4.2) and simultaneously predicts a disease progression risk and a tumor segmentation mask. The DeepMTS is composed of two main components: a segmentation backbone and a cascaded survival network (CSN). The segmentation backbone is a self-designed segmentation network based on 3D U-net [31] (in Section 3.2) and the CSN is a modified 3D DenseNet [48] (in Section 3.3). Deep features are derived from these two components and fed into Fully-Connected (FC) layers for survival prediction. The whole architecture was trained in an end-to-end manner to minimize the combined loss of segmentation loss  $L_{seg}$  and survival prediction loss  $L_{sur}$  (in Section 3.4).

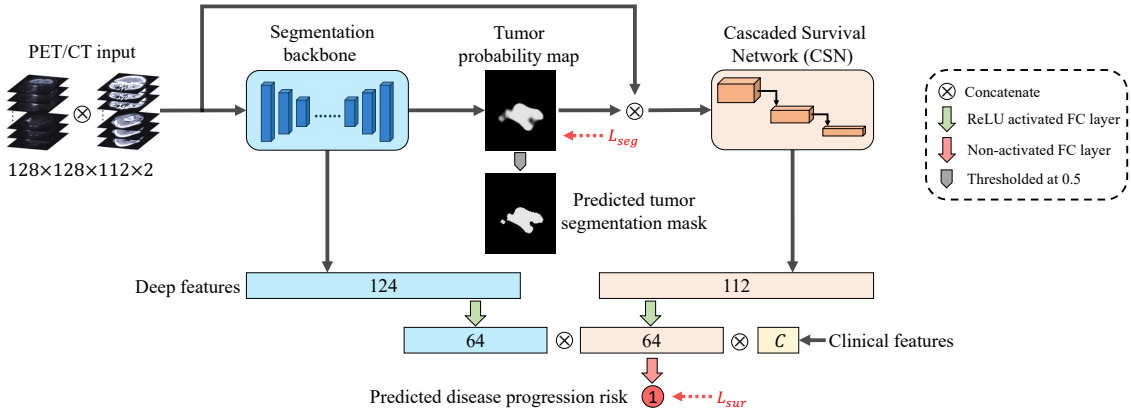


Fig. 2. The workflow of DeepMTS for joint survival prediction and tumor segmentation. It is composed of a self-designed segmentation backbone (blue rectangle) and a cascaded survival network (orange rectangle). Deep features are derived from these two components and fed into FC layers for survival prediction.

Specifically, the preprocessed PET and CT images are first concatenated and fed into the segmentation backbone. Then, the segmentation backbone produces a tumor probability map where each voxel value represents the probability of whether this voxel is located in the tumor regions. Finally, the tumor probability map and the preprocessed PET/CT images are concatenated and fed into the CSN. For the tumor segmentation task, the tumor probability map can be thresholded at 0.5 to obtain a binary tumor segmentation mask. For the survival prediction task, 124 deep features are derived from the downsampling hard-sharing branch of the segmentation backbone and fed into a Rectified Linear Unit (ReLU) [49] activated FC layer with 64 neurons (FC-1); 112 deep features are derived from the CSN and also fed into a ReLU activated FC layer with 64 neurons (FC-2). The FC-1, FC-2, and available clinical features  $C$  (e.g., TNM stage, age, etc.) are concatenated and fed into a non-activated (linear) FC layer with a single neuron (FC-3). The output of FC-3 is the predicted risk of disease progression. Moreover, dropout with 0.5 probability and L2 regularization with 0.1 coefficient are used in all FC layers for regularization.

### 3.2. Segmentation Backbone

Fig. 3 illustrates the architecture of our self-designed segmentation backbone. This self-designed segmentation network is based on 3D U-net [31] and consists of a downsampling hard-sharing branch and an upsampling segmentation branch. As shown in Fig. 3, the left half is the hard-sharing branch that extracts common features for both segmentation and survival prediction tasks; the right half is the segmentation branch that receives the common features through skip connections and performs tumor segmentation. Both the two branches are composed of residual blocks (blue cubes in Fig. 3). Max pooling layers or upsampling layers with the kernel size of  $2 \times 2 \times 2$  are used between adjacent residual blocks for downsampling or upsampling.

A residual block denoted by “ $n \times m$ ” consists of  $n$  stacked convolutional layers with the kernel size of  $3 \times 3 \times 3$  and the kernel number of  $m$ . In this residual block, the 1<sup>st</sup> convolutional layer comes with a non-linear residual connection implemented by a convolutional layer with the kernel size of  $1 \times 1 \times 1$  and the kernel number of  $m$ , while the rest  $n - 1$  convolutional layers come with simple shortcut residual connections. All convolutional layers are followed by Batch Normalization (BN) [50] and ReLU activation. The last residual block is followed by a softmax activated convolutional layer with the kernel size of  $1 \times 1 \times 1$  and the kernel number of 2. The output of the last convolutional layer is the predicted tumor probability map.

Deep features are derived from multi-scale residual blocks in the hard-sharing branch for survival prediction. The output of each residual block is fed into a convolutional layer with the kernel size of  $1 \times 1 \times 1$ , followed by BN, ReLU activation, and a Global Average Pooling (GAP) layer. Finally, a total of 124 deep features are derived from 5 residual blocks. It should be noted that we

used convolutional layers before GAP layers to reduce feature dimensions. Moreover, compared to directly feeding the output of residual blocks into the GAP layers, our design allows for more differences between the features used for different tasks, which might reduce the potential destructive interference [27] existing between the survival prediction task and tumor segmentation task.

### 3.3. Cascaded Survival Network

Fig. 4 illustrates the architecture of the cascaded survival network (CSN). The CSN is a modified version of 3D DenseNet [48]. Firstly, the preprocessed PET/CT and the tumor probability map (from the segmentation backbone) are concatenated and fed into a convolutional layer and a max-pooling layer for downsampling. Then, the feature maps are fed into 3 dense blocks and 3 transition blocks. The 3 dense blocks have 4, 8, and 16 bottleneck blocks, respectively. The bottleneck blocks in the same dense block are densely connected (refer to [48] for more details). Each bottleneck block consists of two convolutional layers with the kernel size of  $1 \times 1 \times 1$  and  $3 \times 3 \times 3$ , respectively. BN and ReLU activation are used before and dropout with 0.05 probability is used after the

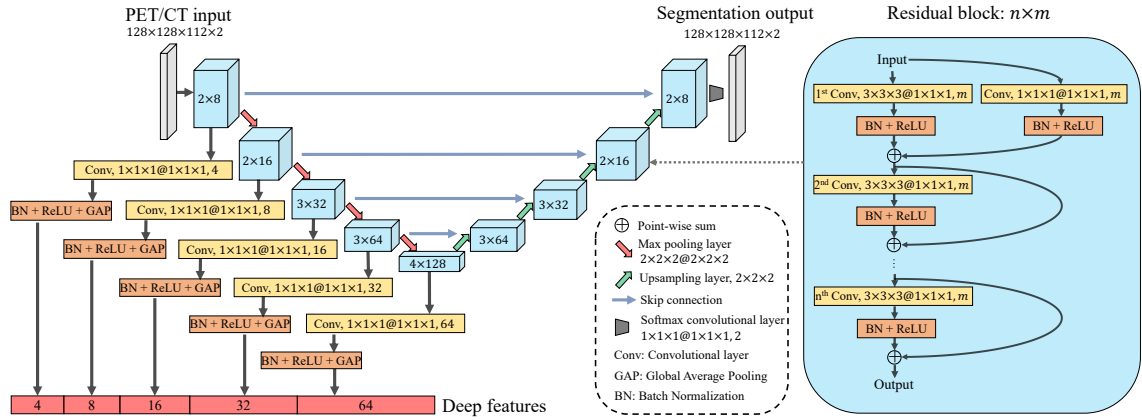


Fig. 3. The architecture of our self-designed segmentation backbone. It is composed of a downsampling hard-sharing branch and an upsampling segmentation branch. The residual block (blue cube) denoted with “ $n \times m$ ” consists of  $n$  stacked convolutional layers with the kernel number of  $m$ . The notation “ $a \times b \times c @ d \times e \times f, m$ ” denotes the kernel size of  $a \times b \times c$ , the stride size of  $d \times e \times f$ , and the kernel number of  $m$ .

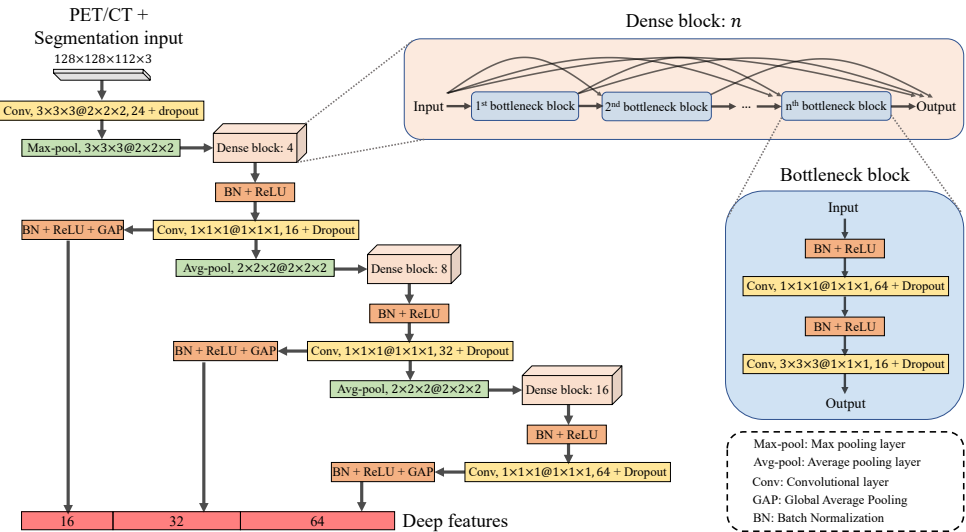


Fig. 4. The architecture of the cascaded survival network (CSN). It is mainly composed of 3 dense blocks. The dense block denoted with “ $n$ ” includes  $n$  densely connected bottleneck blocks. The notation “ $a \times b \times c @ d \times e \times f, m$ ” denotes the kernel size of  $a \times b \times c$ , the stride size of  $d \times e \times f$ , and the kernel number of  $m$ .

convolutional layers in the bottleneck blocks. Each dense block is followed by a transition block consisting of BN, ReLU activation, a convolutional layer with the kernel size of  $1 \times 1 \times 1$ , and dropout with 0.05 probability. The first two transition blocks are followed by an average pooling layer with the kernel size of  $2 \times 2 \times 2$  for downsampling and connecting with later dense blocks. Deep features are derived from multi-scale transition blocks for survival prediction. The output of each transition block is fed into BN, ReLU activation, and a GAP layer. Finally, a total of 112 deep features are derived from 3 transition blocks.

### 3.4. Optimization

Our DeepMTS was trained in an end-to-end manner to minimize a combined loss  $L$  as follows:

$$L = L_{seg} + L_{sur} + \lambda L2_{reg}, \quad (1)$$

where  $L_{seg}$  (Eq.2) is the loss function of the tumor segmentation task,  $L_{sur}$  (Eq.3) is the loss function of the survival prediction task, and  $L2_{reg}$  with the coefficient  $\lambda$  is the L2 regularization term used in FC layers.

For the tumor segmentation task, the  $L_{seg}$  is a Dice loss [32] as follows:

$$L_{seg} = -\frac{2 \sum_i^N p_i g_i}{\sum_i^N p_i^2 + \sum_i^N g_i^2}, \quad (2)$$

where  $p_i \in [0,1]$  is voxels of the predicted tumor probability map,  $g_i \in \{0,1\}$  is the voxels of the ground truth tumor segmentation mask (label), and the sums run over all  $N$  voxels of segmentation space.

For the survival prediction task, we used a Cox negative logarithm partial likelihood loss [46] as the  $L_{sur}$  to handle right-censored survival data, which is shown as follows:

$$L_{sur} = -\frac{1}{N_{E=1}} \sum_{i:E_i=1} (h_i - \log \sum_{j \in \mathcal{H}(T_i)} e^{h_j}), \quad (3)$$

where  $h$  is the predicted risk of disease progression,  $E$  is an event indicator (0 indicates a censored patient and 1 indicates a patient with disease progression),  $T$  is the time of PFS (for  $E = 1$ ) or the time of patient censored (for  $E = 0$ ),  $N_{E=1}$  is the number of patients with disease progression, and  $\mathcal{H}(T_i)$  is a set of patients whose  $T$  is no less than  $T_i$ .

## 4. Experimental Setup

### 4.1. Patients and Datasets

Our training set enrolled 170 patients acquired from Fudan University Shanghai Cancer Center (FUSCC). FUSCC Ethical Committee approved this study, and informed consent was obtained from all enrolled patients. All patients were pathologically confirmed with advanced NPC (TNM stage III or IVa, according to the 8th edition of AJCC guidelines) and received therapeutic regimens at FUSCC according to the National Comprehensive Cancer Network (NCCN) guidelines. Treatment responses were identified by imaging examination according to RECIST 1.1 [51]. The following endpoint was PFS or otherwise censored. PFS was defined as the time from the first day of treatment to the day of disease progression (local relapse, distant metastasis, or death). All patients underwent  $[^{18}\text{F}]$ fluorodeoxyglucose ( $[^{18}\text{F}]$ FDG) PET/CT (Siemens Biograph 16HR, Knoxville, Tennessee, USA) within 4 weeks before treatment and had clinical reports including age, gender, EBV status, histology, BMI, T stage, N stage, TNM stage. We performed univariate Cox analysis for all clinical parameters and only the TNM stage showed significant relevance to PFS ( $P = 0.047$ ). Therefore, only the TNM stage was regarded as a clinical feature and used in our experiments. Moreover, primary tumors were segmented on PET and CT simultaneously using a semi-automatic segmentation algorithm on ITK-SNAP software, and followed by manual adjustment to ensure reliability. This process was performed by two experienced nuclear medicine physicians independently, and they reached a consensus in case of inconsistency.

Our testing set enrolled 23 patients acquired from The Cancer Imaging Archive (TCIA). TCIA released a public dataset including 298 patients with histologically confirmed Head-and-Neck Cancer [52]. In the TCIA dataset, patients were acquired from 4 different centers. All patients underwent  $[^{18}\text{F}]$ FDG PET/CT within a median of 18 days before treatment and had clinical reports including

Table I. Demographic and clinical characteristics of the patients enrolled in the training and testing sets.

Characteristics	Training set,	Testing set
Number of Patients	170	23
Age (year), median (range)	46 (16-78)	61 (18-82)
PFS, Number (%)		
Progression	48 (28.24)	14 (60.87)
Censored	122 (71.76)	9 (39.13)
Gender, Number (%)		
Male	130 (76.47)	19 (82.61)
Female	40 (23.53)	4 (17.39)
T stage, Number (%)		
T1	54 (31.77)	5 (21.74)
T2	21 (12.35)	4 (17.39)
T3	72 (42.35)	9 (39.13)
T4	23 (13.53)	5 (21.74)
N stage, Number (%)		
N0	11 (6.47)	2 (8.70)
N1	34 (20.00)	7 (30.43)
N2	96 (56.47)	9 (39.13)
N3	29 (17.06)	5 (21.74)
TNM stage, Number (%)		
III	121 (71.18)	12 (52.17)
IVa	49 (28.82)	11 (47.83)
Treatment, Number (%)		
None	7 (4.12)	3 (13.04)
Chemotherapy	160 (94.12)	20 (86.96)
Targeted Therapy	26 (15.29)	0 (0)

age, gender, primary site, Human Papilloma Virus (HPV) status, T stage, N stage, and TNM stage. Manually delineated segmentation of primary tumors was given by expert radiation oncologists. Extensive details of the TCIA dataset are available in [53]. A total of 23 patients with advanced NPC were selected from the TCIA dataset and used as our testing set. The selection conditions are: (1) the primary site is nasopharynx and, (2) TNM stage is III or IVa. It should be noted that, in the TCIA dataset, the TNM stage was given according to the 7th edition of AJCC guidelines, so we relabeled it according to the 8th edition of AJCC guidelines for consistency. The demographic and clinical characteristics of the patients enrolled in the training and testing sets were shown in Table I.

#### 4.2. PET/CT Image Preprocessing

Image data was preprocessed through the following steps: (1) All images were resampled into isotropic voxels of unit dimension to ensure comparability, where 1 voxel corresponds to 1 mm<sup>3</sup>. PET/CT images and segmentation masks were resampled via linear interpolation and nearest neighbor interpolation, respectively. (2) PET images were normalized based on body mass. The derived body mass was applied to convert PET images into SUV maps. (3) All images were registered with an anatomical template so that they were located in a relatively fixed position. Specifically, we randomly chose a patient as the template and registered all other patients with it using rigid registration implemented in ANTs [54]. (4) The registered images were cropped into 128 × 128 × 112 Regions-of-Interest (ROIs) by fixed-position cropping. The ROIs covered the whole nasopharynx, so they are suitable for the segmentation and survival prediction of NPC. The fixed cropping positions can be manually decided because all images had been registered and located in a fixed position. (5) The PET/CT ROIs were standardized individually to zero mean and unit variance (Z-score normalization). Finally, the preprocessed PET/CT ROIs were used as the input of models, while the manually delineated tumor segmentation masks were used as ground truth labels for the tumor segmentation task.

#### 4.3. Radiomics Features

For comparison with radiomics-based survival models, we extracted handcrafted radiomics features from the preprocessed PET/CT images, including 19 features from First Order Statistics (FOS), 24 features from Grey-Level Cooccurrence Matrix (GLCM),

16 features from Grey-Level Run Length Matrix (GLRLM), 16 features from Grey-Level Size Zone Matrix (GLSZM), 5 features from Neighboring Grey Tone Difference Matrix (NGTDM), and 16 features based on 3D tumor shape. The manually delineated tumor segmentation masks were used in the feature extraction process to reveal tumor regions. The 16 shape-based features were extracted from the tumor segmentation mask and the remaining  $(19 + 24 + 16 + 16 + 5) = 80$  features (FOS, GLCM, GLRLM, GLSZM, and NGTDM) were extracted from PET and CT tumor regions separately. Moreover, the PET/CT-derived features were recomputed for different wavelet decomposition of PET and CT. Performing low-pass or high-pass wavelet filter along x, y, or z directions resulted in 8 decompositions. Therefore, these features were computed for a total of  $(1 + 8) = 9$  decompositions of PET and CT (including the original ones). Consequently, we derived a total of  $80 \times 9 \times 2 + 16 = 720 \times 2 + 16 = 1456$  radiomics features. This feature extraction process was implemented using Pyradiomics [55], an open-source python package.

#### 4.4. Comparison Methods

Firstly, the proposed DeepMTS was compared to three feature-based survival models. Specifically, redundant radiomics features with Spearman's correlation  $> 0.7$  were first eliminated for dimension reduction, and then the remaining radiomics features and the only available clinical feature (TNM stage) were fed into two popular traditional survival models and one deep survival model:

- Lasso-Cox [37]: an extension of the CPH model [13] using LASSO regression for feature selection.
- RSF (Random Survival Forest) [42]: a tree model that generates an ensemble estimate for survival data.
- DeepSurv [46]: a fully-connected network with a Cox negative logarithm partial likelihood loss (Eq.3).

The Lasso-Cox and RSF were implemented with R packages ("survival", "glmnet", "rms", "Hmisc", and "randomForestSRC"), while the DeepSurv was implemented using the open-source code provided in [46].

Then, the proposed DeepMTS was also compared to three recently proposed end-to-end deep survival models:

- CNN-Survival [23]: a 2D CNN-based survival (CNN-Survival) model that was proposed for survival prediction in pancreatic ductal adenocarcinoma using CT. The CNN-Survival is composed of 6 convolutional layers, 3 max-pooling layers, and 1 FC layer. Right-censored survival data was handled by a discrete-time survival loss proposed by Gensheimer et al. [47].
- MDSN [19]: a 3D multi-modality deep survival network (MDSN) using multi-parametric MRIs. The MDSN is the most recent end-to-end deep model that was proposed for survival prediction in NPC patients. It used a modified 3D DenseNet [48] including 3 dense blocks (53 convolutional layers) and a Cox negative logarithm partial likelihood loss (Eq.3).
- DLPM [24]: a preoperative CT-based deep learning survival prediction model (DLPM) for patients undergoing chest surgery for lung cancer. The DLPM also used a simplified 3D DenseNet [48] including 3 dense blocks (8 convolutional layers) and the discrete-time survival loss proposed by Gensheimer et al. [47].

We strictly followed the references to implement CNN-Survival [23] and MDSN [19]. For DLPM, the open-source code provided in [24] was used for implementation. The MDSN and DLPM took the same input as the DeepMTS, while the CNN-Survival took as input the 2D PET/CT slices multiplied with manually delineated tumor segmentation masks. The output layers of discrete-time survival models (CNN-Survival and DLPM) have 6 neurons, corresponding to the following time intervals: 0–12, 12–24, 24–36, 36–60, 60–84, and 84–120 months. Moreover, for a fair comparison, the clinical feature (TNM stage) was also used. The clinical feature was concatenated with the output of the FC layer (for CNN-Survival) or with the output of the GPA layer (for MDSN and DLPM).

Furthermore, we derived a total of 236 deep features from the trained DeepMTS for comparison with handcrafted radiomics features. The deep features were derived from both the hard-sharing branch (124 features) and the CSN (112 features). Similarly, redundant deep features with Spearman's correlation  $> 0.7$  were first eliminated for dimension reduction, and then the remaining deep features and the clinical feature (TNM stage) were fed into Lasso-Cox, RFS, and DeepSurv.

## 4.5. Experimental Settings

We first compared our proposed DeepMTS with the aforementioned comparison methods (in Section 5.1). Then, we explored the DeepMTS from the following aspects:

- We performed multi-task evaluation (in Section 5.2) to explore how deep multi-task learning improved our DeepMTS. In this experiment, we compared the DeepMTS to five degraded models in which one or more components of DeepMTS were removed: (1) Seg-Backbone: the segmentation backbone was used for tumor segmentation, in which the CSN was removed; (2) Sur-HS: the hard-sharing branch was used for survival prediction, in which the upsampling segmentation branch and CSN were removed; (3) Sur-CasNet: the CSN was used for survival prediction, in which the whole segmentation backbone was removed; (4) MT-HS: the segmentation backbone was used for both tumor segmentation and survival prediction, in which the CSN was removed; (5) MT-CasNet: the segmentation backbone and CSN were used for both survival prediction and tumor segmentation, in which the hard-sharing branch was not used for survival prediction.
- We evaluated different segmentation backbones (in Section 5.3) to explore how our self-designed segmentation backbone contributed to the DeepMTS. In this experiment, we established a baseline DeepMTS, using a widely used 3D U-net [31] as the segmentation backbone, and compared it to the original DeepMTS.
- We analyzed the potential destructive interference existing between the survival prediction and tumor segmentation tasks. In this experiment, we established a baseline MT-HS, removing the convolutional layers between residual blocks and GAP layers, and compared it to the original MT-HS.

## 4.6. Evaluation Metrics

The survival prediction task was evaluated using concordance index (C-index) [56]. The C-index metric measures the consistency between the predicted risk  $h$  and the survival status  $(E, T)$ . It ranges from 0 to 1, where a higher C-index value indicates a more consistent prediction. For discrete-time survival models (CNN-Survival and DLPM), following [23][24][47], their predicted 3-year survival probability (cumulative product to the third time interval) was used to calculate the C-index. For statistical analysis, a two-sided  $P$  value  $< 0.05$  was considered to indicate a statistically significant difference.

The tumor segmentation task was evaluated using Dice Similarity Coefficient (DSC). The DSC metric measures the similarity between the predicted and ground-truth segmentation masks. It also ranges from 0 to 1, where a higher DSC value generally indicates a better segmentation result.

## 4.7. Implementation Details

Our DeepMTS was implemented using Keras with a Tensorflow backend [57] on two 12GB GeForce GTX Titan X GPUs. We used the Adam optimizer [58] with a batch size of 8 to train the DeepMTS for 15000 iterations. The learning rate was 1e-4 initially and then decreased to 5e-5, 1e-5, 1e-6 at the 2500<sup>th</sup>, 5000<sup>th</sup>, 10000<sup>th</sup> training iteration. In the experiments, all models (including all comparison models) were trained and validated through 5-fold cross-validation within the training set. The hyper-parameters were optimized based on the average validation results in the cross-validation. During the training, data augmentation was applied to the input images in real-time to avoid overfitting. The used data augmentation techniques included random translations up to 10 pixels, random rotations up to 5 degrees, and random flipping in the sagittal axis. Furthermore, we sampled an equal number of censored and uncensored samples during the data augmentation process to minimize the problem introduced from our unbalanced dataset. The 5 models trained and validated on 5-fold cross-validation were assembled and then tested on the testing set. The testing results derived from the 5 models were standardized by Z-score normalization and then averaged together to obtain the final testing results. Our implementation code is publicly available at <https://github.com/MungoMeng/DeepMTS>.

## 5. Results

### 5.1. Performance of Survival Prediction

The proposed DeepMTS was compared with existing survival models (described in Section 4.4) for survival prediction, and the C-index results on the training/testing sets are shown in Table II. Among three survival models using radiomics features, the Radiomics features + Lasso-Cox achieved the highest results (C-index: 0.696/0.675), so it was regarded as a traditional benchmark. Among four end-to-end deep survival models, only DeepMTS achieved significantly higher results than the traditional benchmark (C-index: 0.722/0.698 vs 0.696/0.675;  $P = 0.016/0.027$ ), while the CNN-Survival, MDSN, and DLPM failed to outperform the traditional benchmark (C-index: 0.658/0.628, 0.675/0.639, and 0.667/0.642). Furthermore, compared to radiomics features, deep features consistently resulted in significantly higher results in the Lasso-Cox, RFS, and DeepSurv (C-index: 0.711/0.692 vs 0.696/0.675, 0.707/0.688 vs 0.691/0.673, and 0.716/0.694 vs 0.687/0.666;  $P = 0.026/0.045$ ,  $0.034/0.042$ , and  $0.012/0.027$ ).

Table II. C-index results of comparison between the proposed DeepMTS and existing survival models for survival prediction.

Method		Training set (5-fold cross-validation)	Testing set
Radiomics features	+ Lasso-Cox	0.696	0.675
	+ RFS	0.691	0.673
	+ DeepSurv	0.687	0.666
Deep features	+ Lasso-Cox	0.711	0.692
	+ RFS	0.707	0.688
	+ DeepSurv	0.716	0.694
CNN-Survival		0.658	0.628
MDSN		0.675	0.639
DLPM		0.667	0.642
DeepMTS		<b>0.722</b>	<b>0.698</b>

**Bold:** the highest result in each column is in bold.

### 5.2. Multi-task Evaluation

The proposed DeepMTS was compared to five degraded models (Seg-Backbone, Sur-HS, Sur-CasNet, MT-HS, and MT-CasNet) for survival prediction and/or tumor segmentation, and the C-index/DSC results on the cross-validation are shown in Table III. For the survival prediction task, our DeepMTS achieved the highest result (C-index: 0.722) and significantly outperformed the MT-HS and MT-CasNet (C-index: 0.706 and 0.698;  $P = 0.042$  and  $0.017$ ). The MT-HS and MT-CasNet also showed significantly higher results than their single-task counterparts, Sur-HS and Sur-CasNet (without using segmentation; C-index: 0.678 and 0.674;  $P = 0.008$  and  $0.036$ ). We also tried to multiply manually delineated segmentation masks with PET/CT input to reveal tumor regions for the Sur-HS and Sur-CasNet. However, the Sur-HS and Sur-CasNet using manual segmentation showed significantly lower results than their counterparts without using segmentation (C-index: 0.657 and 0.652;  $P = 0.024$  and  $0.020$ ). For the tumor segmentation task,

Table III. Results for multi-task evaluation.

Method	C-index	DSC
Seg-Backbone	/	0.758
Sur-HS (using segmentation)	<b>0.657</b>	/
Sur-HS (no segmentation)	0.678	/
Sur-CasNet (using segmentation)	0.652	/
Sur-CasNet (no segmentation)	0.674	/
MT-HS	0.706	<b>0.763</b>
MT-CasNet	0.698	0.754
DeepMTS	<b>0.722</b>	0.760

**Bold:** the highest result in each column is in bold.

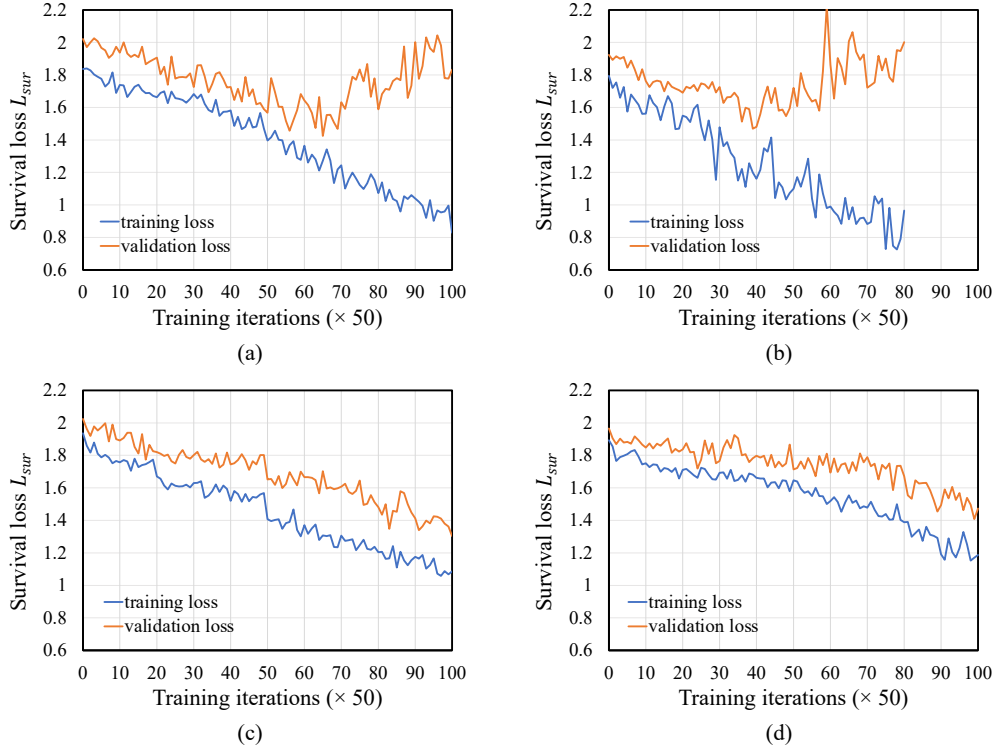


Fig. 5. Training convergence of (a) Sur-HS, (b) Sur-CasNet, (c) MT-HS, and (d) MT-CasNet, which shows the training/validation  $L_{sur}$  with varying number of training iterations.

the MT-HS achieved the highest result (DSC: 0.763) and our DeepMTS gained the second-highest result (DSC: 0.760), followed by Seg-Backbone (DSC: 0.758) and MT-CasNet (DSC: 0.754).

Furthermore, the training convergence of Sur-HS, Sur-CasNet, MT-HS, and MT-CasNet was measured, and the training/validation  $L_{sur}$  with varying number of training iterations is shown in Fig. 5. We identified that overfitting began to occur roughly at the 300<sup>th</sup> and 200<sup>th</sup> training iterations in the Sur-HS and Sur-CasNet, respectively, while the MT-HS and MT-CasNet didn't suffer from the overfitting problem.

### 5.3. Evaluation of Segmentation Backbones

The baseline DeepMTS, using a 3D U-net [31] as the segmentation backbone, was compared to our original DeepMTS for both survival prediction and tumor segmentation, and the C-index/DSC results on the cross-validation are shown in Table IV. For the tumor segmentation task, the Seg-Backbone achieved a higher result than the U-net (DSC: 0.758 vs 0.744). Compared to the U-net backbone, our segmentation backbone consistently contributed to higher results in the MT-HS, MT-CasNet, and DeepMTS (DSC: 0.763 vs 0.747, 0.754 vs 0.740, and 0.760 vs 0.745). For the survival prediction task, compared to the U-net backbone, our segmentation backbone contributed to significantly higher results in the Sur-HS, MT-HS, and DeepMTS (C-index: 0.678 vs 0.655, 0.706 vs 0.680, and 0.722 vs 0.704;  $P = 0.011, 0.021$ , and  $0.039$ ), while there is no significant difference between the original MT-CasNet and its U-net counterpart (C-index: 0.698 vs 0.696,  $P > 0.05$ ).

Furthermore, the training convergence of U-net, Seg-Backbone, baseline DeepMTS, and our DeepMTS was measured and shown in Fig. 6. We identified that our segmentation backbone (Seg-Backbone) showed much faster training convergence than the U-net and contributed to faster training convergence in DeepMTS as well.

Table IV. Results for evaluation of segmentation backbones.

Method	C-index	DSC
U-net	/	0.743
Seg-Backbone (Ours)	/	<b>0.758 (+0.015)</b>
Sur-HS (U-net)	0.655	/
Sur-HS (Ours)	<b>0.678 (+0.023)</b>	/
MT-HS (U-net)	0.680	0.747
MT-HS (Ours)	<b>0.706 (+0.026)</b>	<b>0.763 (+0.016)</b>
MT-CasNet (U-net)	0.696	0.740
MT-CasNet (Ours)	<b>0.698 (+0.02)</b>	<b>0.754 (+0.014)</b>
DeepMTS (U-net)	0.704	0.745
DeepMTS (Ours)	<b>0.722 (+0.018)</b>	<b>0.760 (+0.015)</b>

**Bold:** The results using our segmentation backbone are in bold with the improvements over their U-net counterparts in parentheses.

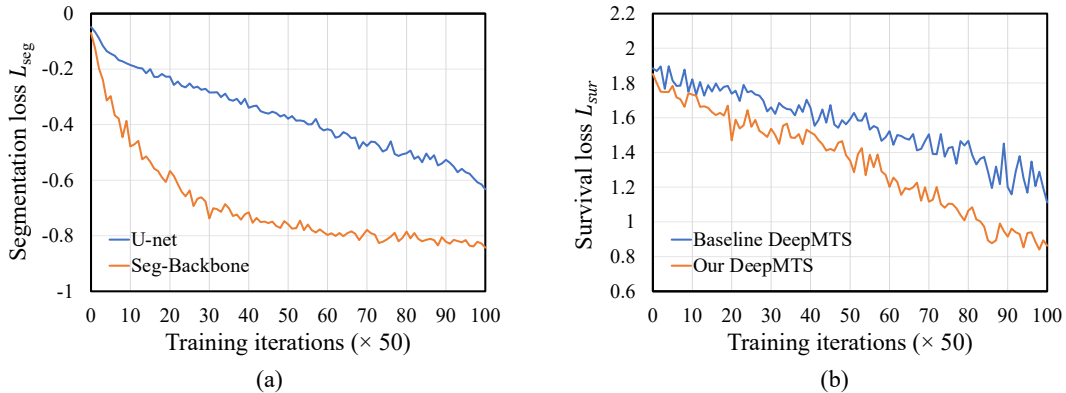


Fig. 6. Training convergence of (a) U-net and Seg-Backbone, and (b) baseline DeepMTS and our DeepMTS, which shows the training  $L_{seg}/L_{sur}$  with varying number of training iterations.

#### 5.4. Analysis of Destructive Interference

The baseline MT-HS, removing the convolutional layers between residual blocks and GAP layers, was compared to our original MT-HS for both survival prediction and tumor segmentation, and the C-index/DSC results on the cross-validation are shown in Table V. The results of Seg-Backbone and Sur-HS, as two benchmarks, were also showed in Table V. As mentioned earlier, our original MT-HS achieved higher results than the Sur-HS and Seg-Backbone. The baseline MT-HS achieved a slightly higher result than the Seg-Backbone (DSC: 0.760 vs 0.758) but showed a significantly lower result than the Sur-HS (C-index: 0.662 vs 0.678;  $P = 0.038$ ). The training convergence of baseline MT-HS and our MT-HS was measured and is showed in Fig. 7. Compared to the baseline MT-HS, our original MT-HS achieved lower training losses for both  $L_{sur}$  and  $L_{seg}$ .

Table V. Results for destructive interference analysis

Method	C-index	DSC
Seg-Backbone	/	0.758
Sur-HS	0.678	/
MT-HS (Baseline)	0.662	0.760
MT-HS (Ours)	<b>0.706</b>	<b>0.763</b>

**Bold:** the highest result in each column is in bold.

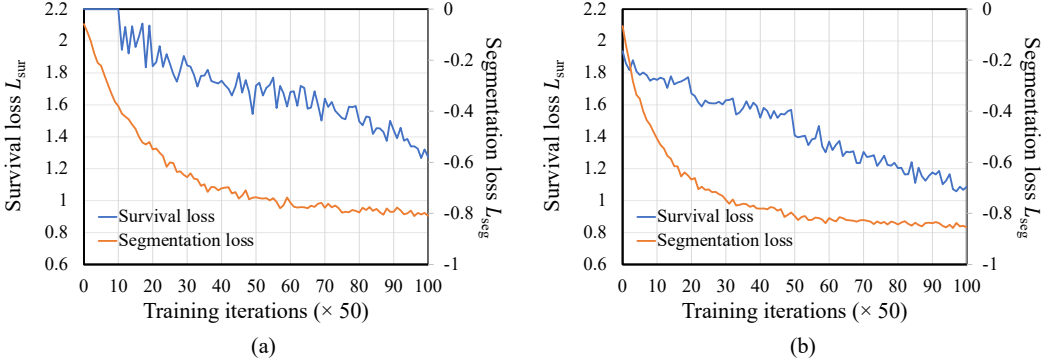


Fig. 7. Training convergence of (a) baseline MT-HS and (b) our MT-HS, which shows the training  $L_{seg}$  and  $L_{sur}$  with varying number of training iterations.

## 6. Discussion

Our main findings are: (1) The proposed DeepMTS outperformed all comparison methods on survival prediction and can extract more discriminative features than manually-defined feature extraction; (2) Deep multi-task learning helped to avoid overfitting and contributed to better performance on survival prediction; (3) Our self-designed segmentation backbone contributed to higher learning efficiency and better performance on both survival prediction and tumor segmentation; (4) There exists destructive interference between the survival prediction task and the tumor segmentation task, but the design of our hard-sharing branch can relieve this interference and contribute to better performance on survival prediction.

In the comparison between the proposed DeepMTS and existing survival models (Table II), the DeepMTS outperformed all comparison methods and showed a significantly higher C-index than the traditional benchmark (Radiomics features + Lasso-Cox), which suggests that the DeepMTS can be a powerful tool for survival prediction. It should be noted that the traditional radiomics-based methods require manual tumor segmentation for both training and testing, while the proposed DeepMTS only require it for training. The MDSN and DLPM failed to outperform the traditional benchmark (Table II). This is attributed to the fact that the MDSN and DLPM were designed for larger datasets (1417 and 640 patients) [19][24], so they are not applicable to our small dataset (170 patients) and suffered from the overfitting problem. The CNN-Survival, as a simple 2D CNN, can apply to our small data, but it still failed to outperform the traditional benchmark as well (Table II). This is likely because the CNN-Survival is a 2D model that makes predictions based on a single slice, thereby losing the prognostic information existing in 3D tumor volumes.

We also found that, compared to handcrafted radiomics features, the deep features derived from the DeepMTS consistently contributed to a significantly higher C-index in the feature-based survival models (Table II). This demonstrates that the DeepMTS can extract more discriminative features than manually-defined feature extraction, which also helps to explain why the DeepMTS can outperform the traditional benchmark. Moreover, we also identified that the end-to-end DeepMTS outperformed the feature-based survival models using deep features (Table II), which is consistent with the findings from Jing et al. [19] and Zhang et al. [23]. This is likely because end-to-end models allow cooperative learning of feature extraction and feature analysis, in which these two parts can better fit with each other.

In the multi-task evaluation (Table III), we identified that the MT-HS achieved a significantly higher C-index than the Sur-HS and a slightly higher DSC than the Seg-Backbone. Moreover, the Sur-HS suffered from the overfitting problem but the MT-HS did not (Fig. 5). These demonstrate that, in the hard-sharing architecture, deep multi-task learning helped to avoid overfitting, enhanced the performance of survival prediction, and did not impose negative impacts on the performance of tumor segmentation. As we have already mentioned, the possible explanations are the tumor segmentation task can guide the model to extract the features related to tumor regions [30] and the segmentation loss has high efficiency in learning from small data [32]. We also identified that the MT-

CasNet achieved a significantly higher C-index than the Sur-CasNet and a slightly lower DSC than the Seg-Backbone (Table III). Also, the Sur-CasNet suffered from the overfitting problem but the MT-CasNet did not (Fig. 5). These demonstrate that, in the cascaded architecture, deep multi-task learning also helped to avoid overfitting, enhanced the performance of survival prediction, but slightly degraded the performance of tumor segmentation. This is likely attributed to three reasons: (1) the segmentation backbone provided supplementary tumor information for the CSN and facilitated survival prediction; (2) the output of the segmentation backbone is variable during training, which imposed inherent data augmentation on the CSN and helped to avoid overfitting; (3) the CSN can make the segmentation target closer to the regions providing prognostic information, while the regions providing prognostic information are not essentially same as the manually delineated tumor regions [29].

The results of the multi-task evaluation (Table III) also showed that the proposed DeepMTS significantly outperformed the MT-HS and MT-CasNet on survival prediction, which suggests that the DeepMTS can benefit from both the hard-sharing branch and the CSN. However, the tumor segmentation performance of DeepMTS was degraded by the CSN and thereby failed to outperform the MT-HS (Table III). Furthermore, we found that the Sur-HS and Sur-CasNet showed significantly degraded performance when their PET/CT input was multiplied with manually delineated segmentation masks (Table III), which suggests that some key prognostic information exists out of tumor regions. Therefore, in the design of CSN, the output of the segmentation backbone was concatenated with PET/CT images and then fed into the CSN. Through this design, the CSN can receive the whole PET/CT and supplementary segmentation information. Moreover, this finding provides an explanation on why our deep features outperformed radiomics features: the deep features derived from our DeepMTS can represent the prognostic information existing in the whole PET/CT, while the radiomics features, extracted from segmented tumor regions, lost the prognostic information existing out of tumor regions.

In the evaluation of segmentation backbones (Table IV), our self-designed segmentation backbone consistently contributed to better performance on tumor segmentation than the U-net backbone, which demonstrates its superior ability of tumor segmentation. Moreover, compared to the U-net backbone, the self-design segmentation backbone contributed to a significantly higher C-index in the Sur-HS and MT-HS (Table IV). This demonstrates that the hard-sharing branch of our segmentation backbone has superior learning capability and can discover more discriminative features for survival prediction. However, our segmentation backbone did not cause a significant difference in the C-index of MT-CasNet, which demonstrates that the CSN is relatively insensitive to the improvement of segmentation backbones. Nevertheless, the DeepMTS still can benefit from the improved hard-sharing branch and achieved better performance on survival prediction by using our segmentation backbone. Furthermore, our segmentation backbone showed much higher learning efficiency than the U-net and contributed to higher learning efficiency in DeepMTS as well (Fig. 6). This is attributed to the fact that residual connections were used in our segmentation backbone to enhance learning efficiency.

Destructive interference (or named as negative transfer) is a phenomenon that increasing the performance on one task will hurt the performance on other tasks [27]. Minimizing destructive interference is a key challenge for multi-task learning. In the analysis of destructive interference (Table V), the baseline MT-HS showed a slightly higher DSC than the Seg-Backbone but a significantly lower C-index than the Sur-HS, which suggests that there exists destructive interference in the baseline MT-HS. In the design of our hard-sharing branch, we inserted a convolutional layer with the kernel size of  $1 \times 1 \times 1$ , between each residual block and each GAP layer, to relieve the destructive interference. This design allows for more differences between the features used for different tasks. Compared to the baseline MT-HS, the MT-HS using our design achieved higher performance (Table V) and lower training losses (Fig. 7) on both two tasks, which demonstrates that the design of our hard-sharing branch indeed relieved the destructive interference and contributed to better performance on survival prediction.

There exist a few limitations in this study. The proposed DeepMTS was trained and validated in a small PET/CT dataset including 170 NPC patients. To ensure reproducibility in real clinical environments, we have measured the statistical significance ( $P$  value) and tested the models in an external testing set acquired from different centers. Nevertheless, a larger dataset is still helpful for further validation and possibly enables better performance. Moreover, our DeepMTS is not bounded to NPC or PET/CT. The DeepMTS can also be applied to other cancers (e.g., head and neck cancer, lung cancer, etc.) or other imaging modalities (e.g., MRI and CT) in our

future study. Finally, we have identified the destructive interference existing between the survival prediction task and the tumor segmentation task, but we only used a very simple design to relieve it. More advanced designs, such as soft-sharing or Cross-Talk architectures [27], can be considered in our future study.

## 7. Conclusion

In this study, we proposed a 3D end-to-end Deep Multi-Task Survival model (DeepMTS) for joint survival prediction and tumor segmentation. Based on our review, this is the first study where deep multi-task learning was introduced for image-derived survival prediction, which provides a potential approach to use deep learning models in scarce medical image data. Furthermore, we designed an efficient segmentation backbone and designed a hybrid multi-task architecture by combining previous hard-sharing multi-task architectures and cascaded multi-task architectures. The experimental results have shown that our designs contributed to higher learning efficiency and better performance on survival prediction.

## References

- [1] Chua MLK, Wee JTS, Hui EP, Chan ATC. Nasopharyngeal carcinoma. *Lancet*. 2016;387(10022):1012-24. doi:10.1016/s0140-6736(15)00055-0.
- [2] Sung H, Ferlay J, Siegel RL, Laversanne M, Soerjomataram I, Jemal A et al. Global cancer statistics 2020: GLOBOCAN estimates of incidence and mortality worldwide for 36 cancers in 185 countries. *CA Cancer J Clin*. 2021. doi:10.3322/caac.21660.
- [3] Huang, Lei, et al. "Longitudinal clinical score prediction in Alzheimer's disease with soft-split sparse regression based random forest." *Neurobiology of aging* 46 (2016): 180-191.
- [4] L.Q. Tang , C.F. Li , J. Li , W.H. Chen , Q.Y. Chen , L.X. Yuan , X.P. Lai , Y. He , Y.X. Xu , D.P. Hu , et al. , Establishment and validation of prognostic nomograms for endemic nasopharyngeal carcinoma, *J. Natl. Cancer Inst.* 108 (1) (2016) .
- [5] Huang CI, Chen LF, Chang SL, Wu HC, Ting WC, Yang CC. Accuracy of a Staging System for Prognosis of 5-Year Survival of Patients With Nasopharyngeal Carcinoma Who Underwent Chemoradiotherapy. *JAMA Otolaryngol Head Neck Surg*. 2017;143(11):1086-91. doi:10.1001/jamaoto.2017.1562.
- [6] Tang X-R, Li Y-Q, Liang S-B, Jiang W, Liu F, Ge W-X et al. Development and validation of a gene expression-based signature to predict distant metastasis in locoregionally advanced nasopharyngeal carcinoma: a retrospective, multicentre, cohort study. *Lancet Oncol*. 2018;19(3):382-93. doi:10.1016/s1470-2045(18)30080-9.
- [7] Lei Y, Li YQ, Jiang W, Hong XH, Zhang Y et al. A Gene-Expression Predictor for Efficacy of Induction Chemotherapy in Locoregionally Advanced Nasopharyngeal Carcinoma. *J Natl Cancer Inst*. 2020. doi:10.1093/jnci/djaa100.
- [8] Chan SC, Hsu CL, Yen TC, Ng SH, Liao CT, Wang HM. The role of 18F-FDG PET/CT metabolic tumour volume in predicting survival in patients with metastatic nasopharyngeal carcinoma. *Oral Oncol*. 2013;49(1):71-8. doi:10.1016/j.oraloncology.2012.07.016.
- [9] Chang KP, Tsang NM, Liao CT, Hsu CL, Chung MJ, Lo CW et al. Prognostic significance of 18F-FDG PET parameters and plasma Epstein-Barr virus DNA load in patients with nasopharyngeal carcinoma. *J Nucl Med*. 2012;53(1):21-8. doi:10.2967/jnumed.111.090696.
- [10] Chen YH, Chang KP, Chu SC, Yen TC, Wang LY, Chang JT et al. Value of early evaluation of treatment response using (18)F-FDG PET/CT parameters and the Epstein-Barr virus DNA load for prediction of outcome in patients with primary nasopharyngeal carcinoma. *Eur J Nucl Med Mol Imaging*. 2019;46(3):650-60. doi:10.1007/s00259-018-4172-3.
- [11] Gillies RJ, Kinahan PE, Hricak H. Radiomics: Images Are More than Pictures, They Are Data. *Radiology*. 2016;278(2):563-77. doi:10.1148/radiol.2015151169.
- [12] Sollini M, Antunovic L, Chiti A, Kirienko M. Towards clinical application of image mining: a systematic review on artificial intelligence and radiomics. *Eur J Nucl Med Mol Imaging*. 2019;46(13):2656-72. doi:10.1007/s00259-019-04372-x.
- [13] Cox, David R. "Regression models and life-tables." *Journal of the Royal Statistical Society: Series B (Methodological)* 34.2 (1972): 187-202.
- [14] Zhang, Bin, et al. "Radiomics features of multiparametric MRI as novel prognostic factors in advanced nasopharyngeal carcinoma." *Cancer Research* 23.15 (2017): 4259-4269.
- [15] Lv, Wenbing, et al. "Radiomics analysis of PET and CT components of PET/CT imaging integrated with clinical parameters: application to prognosis for nasopharyngeal carcinoma." *Molecular imaging and biology* 21.5 (2019): 954-964.

[16] Hosny A, Aerts HJ, Mak RH. Handcrafted versus deep learning radiomics for prediction of cancer therapy response. *Lancet Digit Health.* 2019;1(3):e106-e7. doi:10.1016/s2589-7500(19)30062-7.

[17] Afshar P, Mohammadi A, Plataniotis KN, Oikonomou A, Benali H. From Handcrafted to Deep-Learning-Based Cancer Radiomics: Challenges and Opportunities. *IEEE Signal Processing Magazine.* 2019;36(4):132-60. doi:10.1109/MSP.2019.2900993.

[18] Peng H, Dong D, Fang MJ, Li L, Tang LL, Chen L et al. Prognostic Value of Deep Learning PET/CT-Based Radiomics: Potential Role for Future Individual Induction Chemotherapy in Advanced Nasopharyngeal Carcinoma. *Clin Cancer Res.* 2019;25(14):4271-9. doi:10.1158/1078-0432.CCR-18-3065.

[19] Jing B, Deng Y, Zhang T, Hou D, Li B, Qiang M et al. Deep learning for risk prediction in patients with nasopharyngeal carcinoma using multi-parametric MRIs. *Comput Methods Programs Biomed.* 2020;197:105684. doi:10.1016/j.cmpb.2020.105684.

[20] Matsuo, Koji, et al. "Survival outcome prediction in cervical cancer: Cox models vs deep-learning model." *American journal of obstetrics and gynecology* 220.4 (2019): 381-e1.

[21] Lao, Jiangwei, et al. "A deep learning-based radiomics model for prediction of survival in glioblastoma multiforme." *Scientific reports* 7.1 (2017): 1-8.

[22] Cui, Lei, et al. "A deep learning-based framework for lung cancer survival analysis with biomarker interpretation." *BMC bioinformatics* 21.1 (2020): 1-14.

[23] Zhang, Yucheng, et al. "CNN-based survival model for pancreatic ductal adenocarcinoma in medical imaging." *BMC medical imaging* 20.1 (2020): 1-8.

[24] Kim, Hyungjin, et al. "Preoperative CT-based deep learning model for predicting disease-free survival in patients with lung adenocarcinomas." *Radiology* (2020): 192764.

[25] Peng Y, Bi L, Guo Y, Feng D, Fulham M, Kim J. Deep multi-modality collaborative learning for distant metastases predication in PET-CT soft-tissue sarcoma studies. *Annu Int Conf IEEE Eng Med Biol Soc.* 2019;2019:3658-88. doi:10.1109/embc.2019.8857666.

[26] Zhang, Yu, and Qiang Yang. "A survey on multi-task learning." *IEEE Transactions on Knowledge and Data Engineering* (2021).

[27] Crawshaw, Michael. "Multi-task learning with deep neural networks: A survey." *arXiv preprint arXiv:2009.09796* (2020).

[28] Xue, Zhiyuan, et al. "Radiomics-enhanced multi-task neural network for non-invasive glioma subtyping and segmentation." *International Workshop on Radiomics and Radiogenomics in Neuro-oncology.* Springer, Cham, 2019.

[29] Liu, Jia, et al. "A cascaded deep convolutional neural network for joint segmentation and genotype prediction of brainstem gliomas." *IEEE Transactions on Biomedical Engineering* 65.9 (2018): 1943-1952.

[30] Jin, Cheng, et al. "Predicting treatment response from longitudinal images using multi-task deep learning." *Nature communications* 12.1 (2021): 1-11.

[31] Çiçek, Özgün, et al. "3D U-Net: learning dense volumetric segmentation from sparse annotation." *International conference on medical image computing and computer-assisted intervention.* Springer, Cham, 2016.

[32] Milletari, Fausto, Nassir Navab, and Seyed-Ahmad Ahmadi. "V-net: Fully convolutional neural networks for volumetric medical image segmentation." *2016 fourth international conference on 3D vision (3DV).* IEEE, 2016.

[33] Amyar, Amine, et al. "Multi-task deep learning based CT imaging analysis for COVID-19 pneumonia: Classification and segmentation." *Computers in Biology and Medicine* 126 (2020): 104037.

[34] Cao, Liang, et al. "Multi-task neural networks for joint hippocampus segmentation and clinical score regression." *Multimedia Tools and Applications* 77.22 (2018): 29669-29686.

[35] Mehta, Sachin, et al. "Y-Net: joint segmentation and classification for diagnosis of breast biopsy images." *International Conference on Medical Image Computing and Computer-Assisted Intervention.* Springer, Cham, 2018.

[36] Lee, Changhee, et al. "Deephit: A deep learning approach to survival analysis with competing risks." *Thirty-second AAAI conference on artificial intelligence.* 2018.

[37] Tibshirani, Robert. "The lasso method for variable selection in the Cox model." *Statistics in medicine* 16.4 (1997): 385-395.

[38] Simon, Noah, et al. "Regularization paths for Cox's proportional hazards model via coordinate descent." *Journal of statistical software* 39.5 (2011): 1.

[39] Li, Yan, et al. "Transfer learning for survival analysis via efficient L2, 1-norm regularized Cox regression." *2016 IEEE 16th International Conference on Data Mining (ICDM).* IEEE, 2016.

- [40] Shivaswamy, Pannagadatta K., Wei Chu, and Martin Jansche. "A support vector approach to censored targets." Seventh IEEE International Conference on Data Mining (ICDM 2007). IEEE, 2007.
- [41] Van Belle, Vanya, et al. "Additive survival least-squares support vector machines." *Statistics in Medicine* 29.2 (2010): 296-308.
- [42] Ishwaran, Hemant, et al. "Random survival forests." *The annals of applied statistics* 2.3 (2008): 841-860.
- [43] Mayr, Andreas, and Matthias Schmid. "Boosting the concordance index for survival data—a unified framework to derive and evaluate biomarker combinations." *PloS one* 9.1 (2014): e84483.
- [44] Li, Yan, et al. "A multi-task learning formulation for survival analysis." *Proceedings of the 22nd ACM SIGKDD International Conference on Knowledge Discovery and Data Mining*. 2016.
- [45] Faraggi, David, and Richard Simon. "A neural network model for survival data." *Statistics in medicine* 14.1 (1995): 73-82.
- [46] Katzman, Jared L., et al. "DeepSurv: personalized treatment recommender system using a Cox proportional hazards deep neural network." *BMC medical research methodology* 18.1 (2018): 24.
- [47] Gensheimer, Michael F., and Balasubramanian Narasimhan. "A scalable discrete-time survival model for neural networks." *PeerJ* 7 (2019): e6257.
- [48] Huang, Gao, et al. "Densely connected convolutional networks." *Proceedings of the IEEE conference on computer vision and pattern recognition*. 2017.
- [49] Nair, Vinod, and Geoffrey E. Hinton. "Rectified linear units improve restricted boltzmann machines." *Icml*. 2010.
- [50] Ioffe, Sergey, and Christian Szegedy. "Batch normalization: Accelerating deep network training by reducing internal covariate shift." *International conference on machine learning*. PMLR, 2015.
- [51] Eisenhauer EA, Therasse P, Bogaerts J, Schwartz LH, Sargent D, Ford R et al. New response evaluation criteria in solid tumours: revised RECIST guideline (version 1.1). *Eur J Cancer*. 2009;45(2):228-47. doi:10.1016/j.ejca.2008.10.026.
- [52] Vallières, M. et al. Data from Head-Neck-PET-CT. The Cancer Imaging Archive (2017).
- [53] Vallières, M. et al. Radiomics strategies for risk assessment of tumour failure in head-and-neck cancer. *Scientific Reports* 7, 1–33 (2017).
- [54] Avants, Brian B., Nick Tustison, and Gang Song. "Advanced normalization tools (ANTS)." *Insight j* 2.365 (2009): 1-35.
- [55] Van Griethuysen JJM, Fedorov A, Parmar C, Hosny A, Aucoin N, Narayan V et al. Computational Radiomics System to Decode the Radiographic Phenotype. *Cancer Res*. 2017;77(21):e104-e7. doi:10.1158/0008-5472.Can-17-0339.
- [56] Harrell FE, Lee KL, Mark DB. Multivariable prognostic models: issues in developing models, evaluating assumptions and adequacy, and measuring and reducing errors. *Statistics in Medicine* 1996;15(4):361-87.
- [57] M. Abadi et al. (2016). Tensorflow: Large-scale machine learning on heterogeneous distributed systems. *arXiv preprint arXiv:1603.04467*.
- [58] D. P. Kingma, and J. Ba.(2014). Adam: A method for stochastic optimization .*arXiv preprint arXiv:1412.6980*.